Letter

Measuring the adiabatic non-Hermitian Berry phase in feedback-coupled oscillators

Yaashnaa Singhal,[1,*] Enrico Martello,[2,*] Shraddha Agrawal,[1]
Tomoki Ozawa,[3,†] Hannah Price,[2,‡] and Bryce Gadway[1,§]

[1]*Department of Physics, University of Illinois at Urbana-Champaign, Urbana, Illinois 61801-3080, USA*
[2]*School of Physics and Astronomy, University of Birmingham, Edgbaston, Birmingham B15 2TT, United Kingdom*
[3]*Advanced Institute for Materials Research (WPI-AIMR), Tohoku University, Sendai 980-8577, Japan*

(Received 23 March 2023; revised 8 July 2023; accepted 12 July 2023; published 24 August 2023)

The geometrical Berry phase is key to understanding the behavior of quantum states under cyclic adiabatic evolution. When generalized to non-Hermitian systems with gain and loss, the Berry phase can become complex and should modify not only the phase but also the amplitude of the state. Here, we perform the first experimental measurements of the adiabatic non-Hermitian Berry phase, exploring a minimal two-site $\mathcal{PT}$-symmetric Hamiltonian that is inspired by the Hatano-Nelson model. We realize this non-Hermitian model experimentally by mapping its dynamics to that of a pair of classical oscillators coupled by real-time measurement-based feedback. As we verify experimentally, the adiabatic non-Hermitian Berry phase is a purely geometrical effect that leads to significant amplification and damping of the amplitude also for noncyclical paths within the parameter space even when all eigenenergies are real. We further observe a non-Hermitian analog of the Aharonov-Bohm solenoid effect, observing amplification and attenuation when encircling a region of broken $\mathcal{PT}$ symmetry that serves as a source of imaginary flux. This experiment demonstrates the importance of geometrical effects that are unique to non-Hermitian systems and paves the way towards further studies of non-Hermitian and topological physics in synthetic metamaterials.

DOI: 10.1103/PhysRevResearch.5.L032026

Introduction. Geometrical phases play a fundamental role across physics as they emerge from the cyclic adiabatic evolution of a system, and depend only on certain intrinsic geometrical properties within a given parameter space. In quantum mechanics, a key example of this is the Berry phase [1], which can be related, not only to the quantum geometry of eigenstates but also to important topological invariants, such as the Chern number and winding number [2,3]. Experimentally, the Berry phase has profound effects on material and transport properties, and it underlies Hall effects, polarization, charge pumping, semiclassical dynamics, and many other phenomena [2].

Following its discovery, the Berry phase was generalized to systems with dissipation or gain, in which the Hamiltonian becomes non-Hermitian [4–11]. Interest in such problems has continued to grow, inspired by developments in non-Hermitian experimental platforms, including in photonics [12,13], mechanics [14–20], electric circuits [21,22], and cold atoms [23,24] amongst many others [25–27]. This progress has also been driven by interest in topological systems, in which non-Hermiticity leads to new topological classifications and unusual boundary phenomena [25,27].

Underlying these effects are fundamental differences between Hermitian and non-Hermitian Hamiltonians; this includes that eigenstates can coalesce and become defective at exceptional points, that the left and right eigenfunctions will typically be different from each other, and that the eigenenergies can become complex [13,26]. One important consequence of these differences is that the Berry phase will, in general, become complex- instead of real-valued, implying that the amplitude as well as the phase of a state will vary under adiabatic dynamical evolution [4–7,28–31].

In this paper, we measure the adiabatic non-Hermitian Berry phase, demonstrating how non-Hermiticity leads to gauge-invariant geometrical effects even for noncyclical paths in parameter space. This goes beyond previous experiments which observed the real part of a Berry phase for closed loops around non-Hermitian exceptional points [32–34]; in those cases, the Berry phase was parametric rather than adiabatic as adiabaticity inevitably breaks down when an exceptional point is dynamically encircled [35–37] and geometrical properties have therefore to be reconstructed from eigenmode measurements. In contrast, here we study a two-site $\mathcal{PT}$-symmetric system, in a regime for which the eigenenergies are real and adiabatic evolution is possible. To realize our model, we employ a mapping between quantum evolution and the classical dynamics of a pair of oscillators coupled with real-time measurement-based feedback [20]. We evolve our system adiabatically and experimentally demonstrate that the imaginary part of the Berry phase leads to significant

*These authors contributed equally to this work.
†tomoki.ozawa.d8@tohoku.ac.jp
‡H.Price.2@bham.ac.uk
§bgadway@illinois.edu

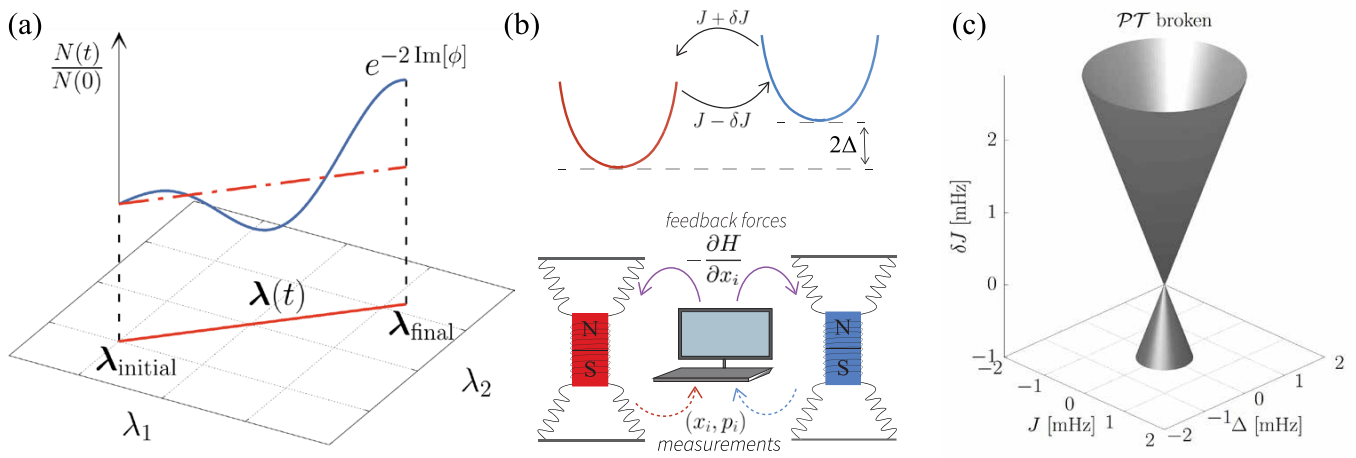

FIG. 1. Exploration of the non-Hermitian Berry phase in the two-site Hatano-Nelson model. (a) In non-Hermitian systems with $\mathcal{PT}$ symmetry, adiabatic paths in parameter space generically results in amplification or attenuation of the time-dependent population $N(t)$. This results directly from the imaginary portion of the adiabatic non-Hermitian Berry phase ϕ acquired by a state along its trajectory. (b) (Top) The Hatano-Nelson (HN) dimer, a minimal non-Hermitian lattice model with nonreciprocal left/right hopping rates $J \pm \delta J$ and an intersite frequency imbalance 2Δ. (Bottom) Implementation of the HN dimer in a mechanical system via measurement-and-feedback. Nonreciprocal coupling between mechanical oscillators, as well as shifts to their resonance frequencies, are realized through applied forces that are responsive to real-time measurements. (c) $\mathcal{PT}$-symmetry breaking phase diagram of the HN dimer. A conical surface of exceptional points in the J-δJ-Δ parameter space separates regions of broken and preserved $\mathcal{PT}$ symmetry, respectively lying inside and outside of the conical surface.

geometrical amplification and damping, which is intrinsically non-Hermitian.

Non-Hermitian Berry phase. Before discussing our experiment, we review the basic theory of non-Hermitian systems [13,26] to motivate the non-Hermitian Berry phase. Various related definitions exist for this phase [4–11]; here, we introduce a formalism that is motivated by physical observables to concisely include all relevant geometrical effects using Berry connections. This definition has the advantage that its imaginary part is manifestly gauge-invariant and is immediately related to measurements of the population. Detailed derivations are given in Ref. [38].

We consider a N-component state vector $|\psi(t)\rangle$, which depends on time t and obeys the Schrödinger-type equation $i\partial_t|\psi(t)\rangle = H(\boldsymbol{\lambda})|\psi(t)\rangle$, where the family of N-by-N non-Hermitian matrices $H(\boldsymbol{\lambda})$ are parameterized by a set of real parameters $\boldsymbol{\lambda} = (\lambda_1, \lambda_2, \dots)$. For a given value of $\boldsymbol{\lambda}$, $H(\boldsymbol{\lambda})$ acts as a non-Hermitian Hamiltonian. It has right and left eigenvectors, denoted by $|R_n(\boldsymbol{\lambda})\rangle$ and $\langle L_n(\boldsymbol{\lambda})|$ respectively, which are generally not complex conjugates of each other [13,26], but which share the same complex eigenvalues $\varepsilon_n(\boldsymbol{\lambda})$, indexed by $n = 1, 2, \dots, N$. Within the parameter space spanned by $\boldsymbol{\lambda}$, four distinct geometrical Berry connections can then be defined [30,39]; however, for the non-Hermitian Berry phase, only the following two Berry connections will be relevant:

$$\mathcal{A}^{LR}_{n,j}(\boldsymbol{\lambda}) \equiv i\langle L_n(\boldsymbol{\lambda})|\partial_{\lambda_j}|R_n(\boldsymbol{\lambda})\rangle / \langle L_n(\boldsymbol{\lambda})|R_n(\boldsymbol{\lambda})\rangle, \tag{1}$$

$$\mathcal{A}^{RR}_{n,j}(\boldsymbol{\lambda}) \equiv i\langle R_n(\boldsymbol{\lambda})|\partial_{\lambda_j}|R_n(\boldsymbol{\lambda})\rangle / \langle R_n(\boldsymbol{\lambda})|R_n(\boldsymbol{\lambda})\rangle. \tag{2}$$

Upon a generalized gauge transformation, which multiplies $|R_n(\boldsymbol{\lambda})\rangle$ and $|L_n(\boldsymbol{\lambda})\rangle$ not just by a phase but also by arbitrary and independent nonzero factors, it can be shown that the following combination of the above Berry connections is invariant [30]:

$$\delta\mathcal{A}^{LR-RR}_{n,j}(\boldsymbol{\lambda}) \equiv \mathcal{A}^{LR}_{n,j}(\boldsymbol{\lambda}) - \mathcal{A}^{RR}_{n,j}(\boldsymbol{\lambda}). \tag{3}$$

It is a distinguishing feature of non-Hermitian systems that gauge-independent quantities can be constructed just from a linear combination of Berry connections; in Hermitian quantum mechanics, the different Berry connections coincide and the gauge-invariant combination $\delta\mathcal{A}^{LR-RR}_{n,i}$ is always zero.

We now consider the adiabatic evolution of a state upon changing the parameter $\boldsymbol{\lambda}(t)$ as a function of time t to extract the non-Hermitian counterpart of the Berry phase [4–7,28–31,40]. Here, we focus on the situation where all the eigenvalues are real and nondegenerate so that we can apply the adiabatic theorem [41,42]. Then if the initial state corresponds to the nth right eigenstate, the state at time t can be written as

$$|\psi(t)\rangle = c(t)\frac{|R_n(\boldsymbol{\lambda}(t))\rangle}{\sqrt{\langle R_n(\boldsymbol{\lambda}(t))|R_n(\boldsymbol{\lambda}(t))\rangle}}, \tag{4}$$

where $c(t)$ is a complex-valued adiabatic factor that the state acquires as $\boldsymbol{\lambda}(t)$ is varied. In defining $c(t)$, we chose to separate out the denominator, as we are interested in physical observables such as the population $N(t)$, which is then given simply by $N(t) \equiv \langle\psi(t)|\psi(t)\rangle = |c(t)|^2$. We note that the final result is independent of the way the state $|\psi(t)\rangle$ is written as a product of a coefficient $c(t)$ and a basis vector, as explained in detail in Ref. [38]. We formally solve the Schrödinger equation $i\partial_t|\psi(t)\rangle = H(\boldsymbol{\lambda}(t))|\psi(t)\rangle = \varepsilon_n(\boldsymbol{\lambda}(t))|\psi(t)\rangle$ by applying $\langle L_n(\boldsymbol{\lambda}(t))|$ from the left, which yields

$$c(t) = c(0)\exp\left[-i\int_0^t dt'\varepsilon_n(\boldsymbol{\lambda}(t')) + i\phi[\mathcal{C}]\right], \tag{5}$$

where the first term in the exponent is the dynamical contribution to the adiabatic factor $c(t)$, whereas the second part is

the non-Hermitian Berry phase that we define by

$$\phi[\mathcal{C}] \equiv \int_{\mathcal{C}} d\boldsymbol{\lambda} \cdot \left(\boldsymbol{\mathcal{A}}_n^{LR}(\boldsymbol{\lambda}) - i\mathrm{Im}\boldsymbol{\mathcal{A}}_n^{RR}(\boldsymbol{\lambda})\right), \tag{6}$$

where $\boldsymbol{\mathcal{A}}_n^{LR}(\boldsymbol{\lambda}) = (\mathcal{A}_{n,1}^{LR}(\boldsymbol{\lambda}), \mathcal{A}_{n,2}^{LR}(\boldsymbol{\lambda}), \dots)$ and similarly for $\boldsymbol{\mathcal{A}}_n^{RR}(\boldsymbol{\lambda})$. The non-Hermitian Berry phase depends on the path $\mathcal{C}$ taken in parameter space and reflects the geometrical structure of the eigenstates, analogous to the well-known Berry phase for Hermitian systems [1,2]. However, unlike the Hermitian Berry phase, the non-Hermitian Berry phase has both real and imaginary parts. In particular, the imaginary part

$$\mathrm{Im}(\phi[\mathcal{C}]) = \int_{\mathcal{C}} d\boldsymbol{\lambda} \cdot \mathrm{Im}\delta\boldsymbol{\mathcal{A}}_n^{LR-RR}(\boldsymbol{\lambda}) \tag{7}$$

depends solely on the imaginary part of $\delta\boldsymbol{\mathcal{A}}_n^{LR-RR}(\boldsymbol{\lambda}) = (\delta\mathcal{A}_{n,1}^{LR-RR}(\boldsymbol{\lambda}), \delta\mathcal{A}_{n,2}^{LR-RR}(\boldsymbol{\lambda}), \dots)$, which is the gauge-invariant combination of Berry connections introduced in Eq. (3). Therefore, it is then immediately obvious that the imaginary part of the non-Hermitian Berry phase is gauge independent even when the path $\mathcal{C}$ is not closed [40]. On the other hand, the real part of the Berry phase is gauge invariant only when the path $\mathcal{C}$ forms a closed path, just like in the Hermitian case [2]. When the eigenvalues are all real, the evolution of the population [as depicted in Fig. 1(a)] is thus determined purely by the imaginary part of the Berry phase as

$$N(t) = |c(t)|^2 = N(0)\exp\left[-2\mathrm{Im}(\phi[\mathcal{C}])\right], \tag{8}$$

which is directly observable in our experiment.

Experimental setup. To experimentally explore the effects of non-Hermitian geometry, we implement the simple two-site model Hamiltonian

$$H = \begin{pmatrix} -\Delta & J+\delta J \\ J-\delta J & \Delta \end{pmatrix}, \tag{9}$$

as depicted in Fig. 1(b). The elements of H have units of frequency, consistent with the aforementioned Schrödinger-type equation describing the system dynamics. Physically, the real parameters Δ, J, and δJ relate to relevant frequency shifts of (Δ) and hopping rates between $(J \pm \delta J)$ the oscillators. This model is inspired by the Hatano-Nelson model for a 1D lattice [43], which has nonreciprocal hoppings between neighboring lattice sites and which can exhibit nontrivial topology and the non-Hermitian skin effect [27]. The eigenvalues of Eq. (9) are given by $\varepsilon_\pm = \pm\sqrt{\Delta^2 + J^2 - \delta J^2}$, which means that the two eigenvalues are both real when $\Delta^2 + J^2 > \delta J^2$, corresponding to the $\mathcal{PT}$-symmetric region. If $\Delta^2 + J^2 = \delta J^2$, the eigenvalues coalesce at an exceptional point; within the parameter space of $(\Delta, J, \delta J)$, the surface of exceptional points corresponds to a double cone, with its apex at the origin [11], as shown in Fig. 1(c).

The gauge-invariant combinations of the Berry connections within the $\mathcal{PT}$-symmetric region [cf. Eq. (3)] are all purely imaginary, and they diverge as we approach the $\mathcal{PT}$-symmetry breaking transition, where adiabaticity breaks down. (Analytical expressions of the Berry connections and associated Berry curvatures are derived in Ref. [38], and can be interpreted in terms of a complex hyperbolic pseudomagnetic monopole in parameter space [11,31].) This in turn means that the only nonvanishing part of the non-Hermitian Berry phase [Eq. (6)] is purely imaginary and therefore gauge-invariant for any path.

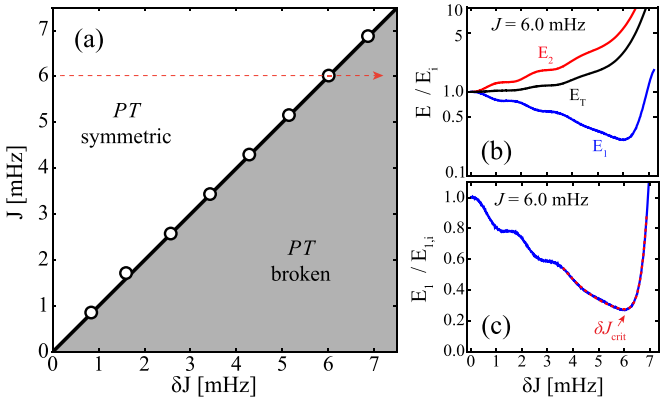

FIG. 2. $\mathcal{PT}$-symmetry breaking phase diagram of the unbiased ($\Delta = 0$) Hatano-Nelson dimer. (a) White points mark the experimentally measured exceptional points (EPs). Critical δJ values for these points are determined by detecting the breakdown of adiabaticity as the EP is crossed. (b) Experimental energy dynamics of prepared eigenstates along the ramp of δJ [dashed red line in (a)] for $J = 6.0$ mHz. The measured energy at site 1 decays (while the site 2 and total energy grow) until the EP is reached at $\delta J \sim J$. Here, we plot the site 1 (E_1), site 2 (E_2), and total energy (E_T) normalized to their respective initial values (E_i). (c) Crossing of the EP is marked by the onset of growth of the otherwise decaying site 1. The red dashed line is an empirical fit to the data, with the fit minimum defining δJ_{crit}. Here, we plot the energy in oscillator 1 normalized to its initial value ($E_1/E_{1,i}$).

To explore the two-site Hatano-Nelson model, we construct a synthetic mechanical lattice consisting of two classical oscillators artificially coupled by real-time feedback measurements, based on our approach reported in Ref. [20]. The essential idea of this scheme is to map the Heisenberg equations of motion for a desired tight-binding quantum Hamiltonian onto Newtons equations of motion for classical oscillators in phase-space within a rotating wave-approximation [44,45]. As discussed in [20], the use of real-time feedback then means that almost any two level non-Hermitian Hamiltonian can be realized with this setup. Here, we use self- and cross-feedback between the oscillators to realize the Hamiltonian described in Eq. (9), as depicted at the bottom of Fig. 1(b). Self-feedback terms proportional to the oscillator positions ($F_i \propto x_i$) allow us to shift their frequencies by $\pm\Delta$ from a nominal starting value of $f_0 \approx 3.05$ Hz. Cross-feedback forces ($F_i \propto x_j$) allow us to introduce independent left-to-right and right-to-left hopping terms $J \pm \delta J$, with no intrinsic limitation to reciprocal energy exchange. By applying self-feedback terms proportional to the oscillator's momenta ($F_i \propto p_i$), we cancel the oscillator's natural damping and explore coherent dynamics for well over 1000 s (>3000 periods). These long timescales are crucial to performing the first explorations of adiabatic response in a non-Hermitian system. Beyond single-body (quadratic, in the operator sense) terms, we additionally apply higher-order feedback to cancel nearly all native quartic nonlinearities. However, small residual nonlinearities remain, serving to, e.g., cap the energy growth in cases of broken $\mathcal{PT}$ symmetry.

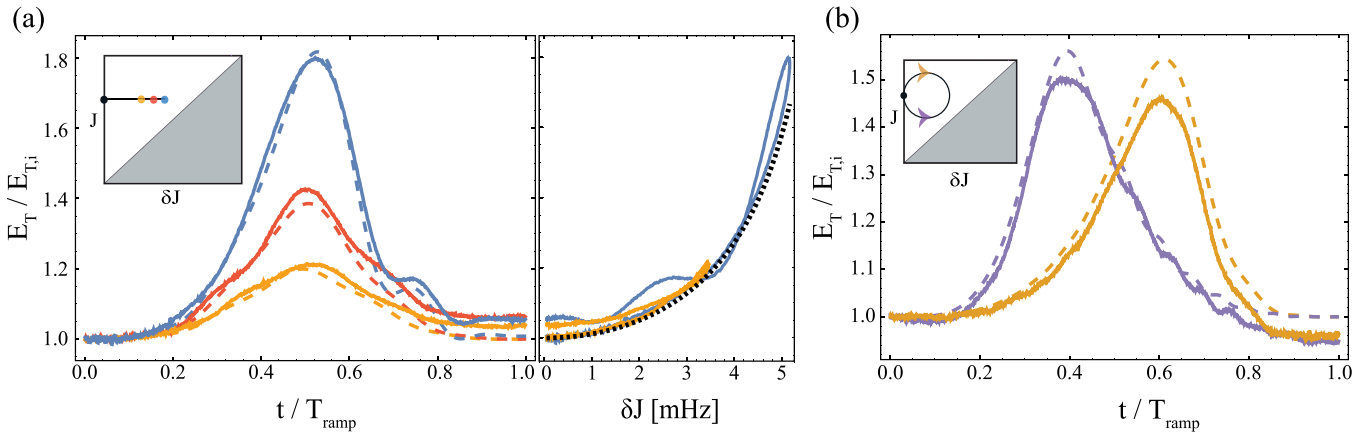

FIG. 3. Geometric energy amplification and attenuation in the Hatano-Nelson dimer. (a) (Left) Dynamics of the total energy $E_T = E_1 + E_2$ for adiabatic transformations (normalized to its initial value $E_{T,i}$). (Inset) Path of the adiabatic transformation, for fixed $J = 6.5$ mHz, ramping from $\delta J = 0$ to/from different maximum values of $\delta J_{\max} = 3.4$ (yellow), 4.3 (red), and 5.2 mHz (blue). (Right) Plot of the total energy vs the instantaneous δJ value, for the yellow and blue paths. The black dotted line shows the expected parametric dependence of $E_T/E_{T,i}$ on δJ for fully adiabatic evolution under H. (b) Dynamics of E_T for CW (purple) and CCW (gold) paths as specified by the inset, centered at $(J, \delta J) = (6.5, 2.2)$ mHz and having a radius of 2.2 mHz. The colored dashed lines in the main panels relate to the time-dependent solutions of the Schrödinger-type equation based on evolution under the ideal HN model, including nonadiabatic effects caused from finite ramp durations of $T_{\text{ramp}} = 500$ for (a) and 1000 s for (b).

Results. We first experimentally establish the $\mathcal{PT}$-symmetry breaking phase diagram of the canonical two-site Hatano-Nelson model, with tunable reciprocal (J) and nonreciprocal (δJ) components of the real-valued intersite hopping, but with no intersite bias ($\Delta = 0$). In this case, for fixed J, an exceptional point and $\mathcal{PT}$-symmetry breaking phase transition are encountered at $\delta J = J$, as previously demonstrated with this platform by spectral analysis in Ref. [20]. In the full $(J, \delta J)$ parameter space, there are two distinct regions of conserved and broken $\mathcal{PT}$ symmetry, denoted by white and grey in Fig. 2(a). We experimentally determine the exceptional line separating these regions by probing the breakdown of adiabaticity and the rapid onset of energy growth as states cross over into the $\mathcal{PT}$-broken region, as shown in Fig. 2(b). We prepare eigenmodes of the symmetric double-well for various fixed values of the reciprocal hopping J, and then linearly ramp δJ from 0 to 1.2 J over 400 s. We establish the exceptional points (white circles) by determining the instantaneous δJ values for which there begins to be energy growth at the otherwise decaying first site, as shown in Fig. 2(c). Here, an observable proportional to the i^{th} oscillator energy $E_i(t)$ is reconstructed from the measured x_i and p_i signals [20]. We can then associate the oscillators' energy dynamics with relative changes in the macroscopic mechanical energy population $N_i(t) \sim E_i(t)/hf_0$.

We now restrict ourselves to the $\mathcal{PT}$-symmetric region of Fig. 2(a), exploring the adiabatic gauge invariant non-Hermitian Berry phase acquired (via the energy dynamics of prepared eigenmodes), as we slowly evolve along controlled paths in parameter space. In Fig. 3(a), we first prepare our system as an eigenmode of the symmetric double well for a fixed reciprocal hopping $J = 6.45$ mHz, and then we smoothly vary the asymmetric hopping as $\delta J(t) = \delta J_{\max} \sin^2(\pi t/T_{\text{ramp}})$ over a time $T_{\text{ramp}} = 500$ s. From the left inset, this corresponds to a closed linear path in parameter space from the black dot at $\delta J = 0$ to one of the colored dots (representing different values of $\delta J_{\max}$), and back. It is seen in Fig. 3(a) that the total energy increases as the trajectory moves closer to the exceptional line, with the blue ($\delta J_{\max} = 5.16$ mHz) path showing the largest gain. For such a trajectory, the energy in the system is determined by the instantaneous δJ value, as confirmed by the parametric collapse of the energy vs. δJ for the yellow and blue curves, shown in the right plot. To note, slight wiggles in both the data (solid lines) and the numerical simulation curves (dashed lines that include effects of the finite ramp duration), arise primarily from nonadiabatic deviations accumulated near the exceptional line. However, for all curves the total energy returns to near its initial value at the end of the trajectories, consistent with adiabatic evolution along a time-reversed path that encloses zero non-Hermitian flux.

In Fig. 3(b), we start from the same conditions but now move along closed circular loops by also varying the symmetric hopping term J by a sinusoidal function over a time period of 1000 s. Coordination between the variation of J and δJ allows us to make either clockwise or counterclockwise paths in parameter space (inset). The energy dynamics curves for the two path directions are essentially (up to small nonadiabatic corrections) mirrored versions of each other with respect to the time midpoint $T_{\text{ramp}}/2$, as the gauge-invariant Berry phase accumulated from the common starting point is again uniquely determined by the instantaneous position in parameter space. This is consistent with the fact that these finite-area paths enclose *zero* non-Hermitian Berry phase. To note, the curves in Figs. 3(a) and 3(b) do exhibit percent level gain and loss over their respective evolution times of 500 and 1000 s, stemming from residual loss and gain terms at the scale of a few μHz.

We now explore closed paths in parameter space that enclose a region of broken $\mathcal{PT}$ symmetry, and which correspondingly acquire a finite non-Hermitian Berry phase. We accomplish this by introducing a site-to-site energy bias (Δ).

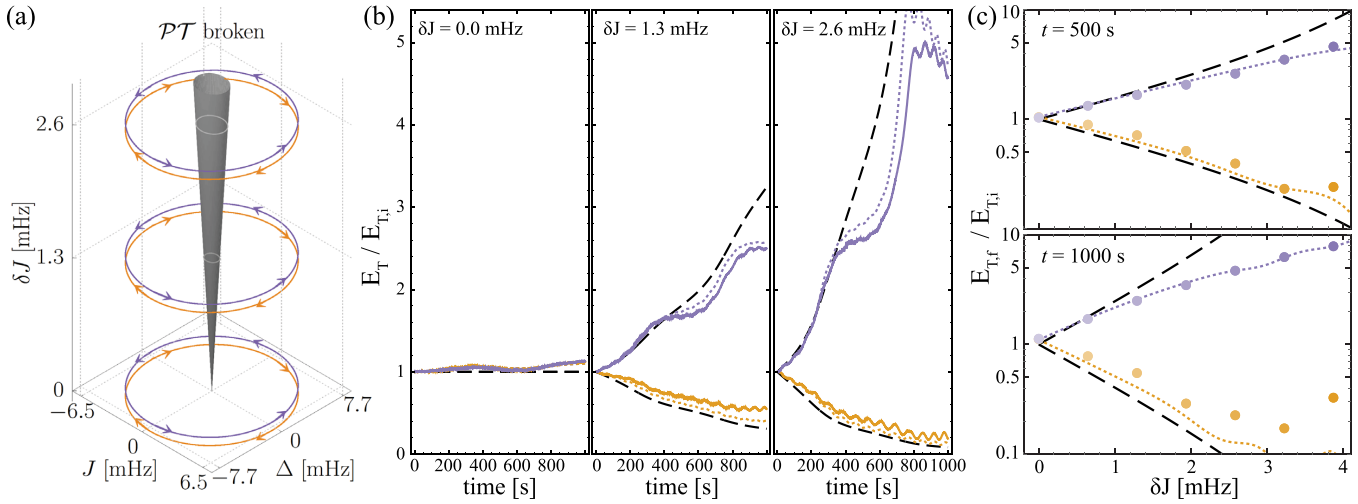

FIG. 4. Cyclic amplification and attenuation along adiabatic paths enclosing PT-broken sources of non-Hermitian Berry phase. (a) Illustration of the paths traversed in parameter space. For trajectories in the J-Δ plane at fixed and finite δJ, the paths enclose a conical $\mathcal{PT}$-broken region that acts as a source of non-Hermitian Berry flux. (b) Dynamics of the total energy $E_T = E_1 + E_2$ for CCW (purple) and CW (gold) paths in the J-Δ plane as specified in panel (a), shown for three values of the tunneling asymmetry δJ. The solid purple (gold) lines are the measured trajectories from experiment for CCW (CW) paths. The long-dashed and short-dashed lines are theory comparisons, described below. (c) Ratio of the final total energy $E_{T,f}$ to the initial total energy $E_{T,i}$ as a function of the tunneling asymmetry δJ. The upper and lower panels show the energy ratios for one half cycle and one full cycle, respectively. The purple (gold) points are the experimentally measured ratios for the CCW (CW) paths (with error bars smaller than the data points) and the long-dashed and short-dashed lines are theory comparisons. For (b) and (c), the black long-dashed lines are the analytical predictions (detailed in Ref. [38]) for the amplification/attenuation under fully adiabatic evolution according to Eq. (9). The dotted lines are the trajectories determined by numerical simulation of the experimental ramping procedure, also incorporating weak nonlinear contributions that serve to capture the saturation observed for large amplification (detailed in Ref. [38]).

To recall, the exceptional surface in the full $(\Delta, J, \delta J)$ parameter space of Eq. (9) corresponds to a double cone with an apex at the origin [11]. As depicted in Fig. 4(a), this admits closed paths within the $\mathcal{PT}$-symmetric region that enclose areas of broken $\mathcal{PT}$ symmetry. The $\mathcal{PT}$-broken region can, in a sense, serve as a source of non-Hermitian Berry flux, analogous to how a magnetic solenoid serves as a source of flux in the canonical Aharonov-Bohm thought experiment [46]. Indeed, our procedure can be viewed as measuring the imaginary Aharonov-Bohm phase in parameter space.

We explore the dynamics of the total energy E_T as we traverse counterclockwise (CCW) and clockwise (CW) paths in the J-Δ plane, starting from several fixed values of δJ. We start by preparing eigenmodes of the system with $J = 0$ and then ramp, over 1000 s, about an ellipse in the J-Δ parameter space as displayed in Fig. 4(a). As we see from Fig. 4(b), the dynamics of the total energy are strongly dependent on δJ. In the fully symmetric case, $\delta J = 0$, we find no significant change to the total oscillator energy, as expected from the lack of an enclosed $\mathcal{PT}$-broken region. For increasing values of δJ, we find that the CCW (CW) paths in parameter space lead to an increasing growth (decay) of the energy upon completing one cycle. Figure 4(c) summarizes the δJ-dependence of the measured gain (attenuation) of the total energy experienced upon completing one cycle in the CCW (CW) direction. The near-exponential dependence of the measured gain (attenuation) with δJ is in qualitative agreement with the expected variation of the acquired non-Hermitian Berry phase for cyclic paths. The non-Hermitian Berry phase accumulated around such paths grows with the size of the $\mathcal{PT}$-broken region, having a form that is nearly proportional to δJ, as presented in Ref. [38]. For the experimentally traversed path in the CCW (CW) direction, the system picks up a negative (positive) contribution of this imaginary phase, and the state of the oscillators thus experiences a corresponding growth (decay) in its energy. At short times or for small values of the hopping asymmetry δJ, the observed amplification and attenuation are in fair agreement with the analytical form expected based on pure geometric contributions of an imaginary Berry phase. However, clear deviations can be found, most prominently in situations where very large growth of the total energy are expected (CCW orbits for large δJ values). On physical grounds, deviations from the expected response can be expected for very large oscillator displacements due to natural anharmonicities. We qualitatively capture the observed saturation of growth by comparing to a dynamical evolution that incorporates small but non-negligible (empirical) nonlinear contributions, described further in Ref. [38].

Conclusion. We have experimentally measured the non-Hermitian Berry phase for adiabatic evolution in a two-site Hatano-Nelson model. We have demonstrated significant geometrical contributions to amplification and damping along both closed and open paths, and shown that these effects are observable in a synthetic mechanical metamaterial. Going further, we will be able to add different types of nonlinearities to the two-site Hatano-Nelson model, allowing us to explore the interplay of interactions with $\mathcal{PT}$ symmetry [47,48]. As active mechanical metamaterials are scaled up to larger systems with dozens of oscillators, they will enable controllable explorations of the effects of quantum geometry and

topology in non-Hermitian Chern insulators, such as, for example, the anomalous velocity contributions predicted to arise from the non-Hermitian Berry phase [30] and the breakdown of the canonical bulk-boundary correspondence of Hermitian models [49–51].

Acknowledgments. We thank Barry Bradlyn for helpful discussions. This material (Y.S., S.A., B.G.) is based upon work supported by the National Science Foundation under Grant No. 1945031. Y.S. acknowledges support by the Philip J. and Betty M. Anthony Undergraduate Research Award and the Jeremiah D. Sullivan Undergraduate Research Award of the UIUC Department of Physics. T.O. acknowledges support from JSPS KAKENHI Grant No. JP20H01845, JST PRESTO Grant No. JPMJPR19L2, JST CREST Grant No. JPMJCR19T1, and RIKEN iTHEMS. E.M. and H.M.P. are supported by the Royal Society via Grants No. UF160112, No. RGF\EA\180121, and No. RGF\R1\180071. E.M. and H.M.P. are also supported by the Engineering and Physical Sciences Research Council (Grant No. EP/W016141/1). This work was also supported by the BRIDGE Seed Fund for collaboration between the University of Birmingham and the University of Illinois at Urbana-Champaign.

[1] M. V. Berry, Quantal phase factors accompanying adiabatic changes, Proc. R. Soc. London A **392**, 45 (1984).
[2] D. Xiao, M.-C. Chang, and Q. Niu, Berry phase effects on electronic properties, Rev. Mod. Phys. **82**, 1959 (2010).
[3] M. Z. Hasan and C. L. Kane, Colloquium: Topological insulators, Rev. Mod. Phys. **82**, 3045 (2010).
[4] J. C. Garrison and E. M. Wright, Complex geometrical phases for dissipative systems, Phys. Lett. A **128**, 177 (1988).
[5] G. Dattoli, R. Mignani, and A. Torre, Geometrical phase in the cyclic evolution of non-Hermitian systems, J. Phys. A: Math. Gen. **23**, 5795 (1990).
[6] F. Keck, H. J. Korsch, and S. Mossmann, Unfolding a diabolic point: A generalized crossing scenario, J. Phys. A: Math. Gen. **36**, 2125 (2003).
[7] S.-D. Liang and G.-Y. Huang, Topological invariance and global berry phase in non-Hermitian systems, Phys. Rev. A **87**, 012118 (2013).
[8] A. Mondragón and E. Hernández, Berry phase of a resonant state, J. Phys. A: Math. Gen. **29**, 2567 (1996).
[9] M. V. Berry and M. R. Dennis, The optical singularities of birefringent dichroic chiral crystals, Proc. R. Soc. London A **459**, 1261 (2003).
[10] M. V. Berry, Physics of nonhermitian degeneracies, Czech. J. Phys. **54**, 1039 (2004).
[11] A. I. Nesterov and F. A. de la Cruz, Complex magnetic monopoles, geometric phases and quantum evolution in the vicinity of diabolic and exceptional points, J. Phys. A: Math. Theor. **41**, 485304 (2008).
[12] A. Guo, G. J. Salamo, D. Duchesne, R. Morandotti, M. Volatier-Ravat, V. Aimez, G. A. Siviloglou, and D. N. Christodoulides, Observation of $\mathcal{PT}$-Symmetry Breaking in Complex Optical Potentials, Phys. Rev. Lett. **103**, 093902 (2009).
[13] Ş. K. Özdemir, S. Rotter, F. Nori, and L. Yang, Parity–time symmetry and exceptional points in photonics, Nat. Mater. **18**, 783 (2019).
[14] C. Coulais, D. Sounas, and A. Alù, Static non-reciprocity in mechanical metamaterials, Nature (London) **542**, 461 (2017).
[15] M. Brandenbourger, X. Locsin, E. Lerner, and C. Coulais, Non-reciprocal robotic metamaterials, Nat. Commun. **10**, 4608 (2019).
[16] C. Scheibner, W. T. M. Irvine, and V. Vitelli, Non-Hermitian Band Topology and Skin Modes in Active Elastic Media, Phys. Rev. Lett. **125**, 118001 (2020).
[17] C. Scheibner, A. Souslov, D. Banerjee, P. Surowka, W. T. M. Irvine, and V. Vitelli, Odd elasticity, Nat. Phys. **16**, 475 (2020).
[18] D. Zhou and J. Zhang, Non-Hermitian topological metamaterials with odd elasticity, Phys. Rev. Res. **2**, 023173 (2020).
[19] A. Ghatak, M. Brandenbourger, J. van Wezel, and C. Coulais, Observation of Non-Hermitian topology and its bulk–edge correspondence in an active mechanical metamaterial, Proc. Natl. Acad. Sci. USA (2020).
[20] R. Anandwade, Y. Singhal, S. N. M. Paladugu, E. Martello, M. Castle, S. Agrawal, E. Carlson, C. Battle-McDonald, T. Ozawa, H. M. Price, and B. Gadway, Synthetic mechanical lattices with synthetic interactions, Phys. Rev. A **108**, 012221 (2023).
[21] Y. Choi, C. Hahn, J. W. Yoon, and S. H. Song, Observation of an anti-PT-symmetric exceptional point and energy-difference conserving dynamics in electrical circuit resonators, Nat. Commun. **9**, 2182 (2018).
[22] T. Helbig, T. Hofmann, S. Imhof, M. Abdelghany, T. Kiessling, L. W. Molenkamp, C. H. Lee, A. Szameit, M. Greiter, and R. Thomale, Generalized bulk–boundary correspondence in non-Hermitian topolectrical circuits, Nat. Phys. **16**, 747 (2020).
[23] W. Gou, T. Chen, D. Xie, T. Xiao, T.-S. Deng, B. Gadway, W. Yi, and B. Yan, Tunable Nonreciprocal Quantum Transport through a Dissipative Aharonov-Bohm Ring in Ultracold Atoms, Phys. Rev. Lett. **124**, 070402 (2020).
[24] J. Li, A. K. Harter, J. Liu, L. de Melo, Y. N. Joglekar, and L. Luo, Observation of parity-time symmetry breaking transitions in a dissipative Floquet system of ultracold atoms, Nat. Commun. **10**, 855 (2019).
[25] C. Coulais, R. Fleury, and J. van Wezel, Topology and broken Hermiticity, Nat. Phys. **17**, 9 (2021).
[26] Y. Ashida, Z. Gong, and M. Ueda, Non-Hermitian physics, Adv. Phys. **69**, 249 (2020).
[27] E. J. Bergholtz, J. C. Budich, and F. K. Kunst, Exceptional topology of non-Hermitian systems, Rev. Mod. Phys. **93**, 015005 (2021).
[28] S. Longhi, Bloch oscillations in complex crystals with $\mathcal{PT}$ symmetry, Phys. Rev. Lett. **103**, 123601 (2009).
[29] R. Hayward and F. Biancalana, Complex Berry phase dynamics in $\mathcal{PT}$-symmetric coupled waveguides, Phys. Rev. A **98**, 053833 (2018).
[30] N. Silberstein, J. Behrends, M. Goldstein, and R. Ilan, Berry connection induced anomalous wave-packet dynamics in non-Hermitian systems, Phys. Rev. B **102**, 245147 (2020).
[31] R. Hayward and F. Biancalana, Monopole-antimonopole instability in non-Hermitian coupled waveguides, Phys. Rev. A **101**, 043846 (2020).

[32] C. Dembowski, H.-D. Gräf, H. L. Harney, A. Heine, W. D. Heiss, H. Rehfeld, and A. Richter, Experimental Observation of the Topological Structure of Exceptional Points, Phys. Rev. Lett. **86**, 787 (2001).

[33] C. Dembowski, B. Dietz, H.-D. Gräf, H. L. Harney, A. Heine, W. D. Heiss, and A. Richter, Encircling an exceptional point, Phys. Rev. E **69**, 056216 (2004).

[34] T. Gao, E. Estrecho, K. Y. Bliokh, T. C. H. Liew, M. D. Fraser, S. Brodbeck, M. Kamp, C. Schneider, S. Höfling, Y. Yamamoto, F. Nori, Y. S. Kivshar, A. Truscott, R. Dall, and E. A. Ostrovskaya, Observation of non-Hermitian degeneracies in a chaotic exciton-polariton billiard, Nature (London) **526**, 554 (2015).

[35] R. Uzdin, A. Mailybaev, and N. Moiseyev, On the observability and asymmetry of adiabatic state flips generated by exceptional points, J. Phys. A: Math. Theor. **44**, 435302 (2011).

[36] M. V. Berry, Optical polarization evolution near a Non-Hermitian degeneracy, J. Opt. **13**, 115701 (2011).

[37] J. Doppler, A. A. Mailybaev, J. Böhm, U. Kuhl, A. Girschik, F. Libisch, T. J. Milburn, P. Rabl, N. Moiseyev, and S. Rotter, Dynamically encircling an exceptional point for asymmetric mode switching, Nature (London) **537**, 76 (2016).

[38] See Supplemental Material at http://link.aps.org/supplemental/10.1103/PhysRevResearch.5.L032026 for a more detailed discussion and analysis of the theoretical model and for a more detailed description of the data analysis.

[39] H. Shen, B. Zhen, and L. Fu, Topological Band Theory for Non-Hermitian Hamiltonians, Phys. Rev. Lett. **120**, 146402 (2018).

[40] S. Massar, Applications of the complex geometric phase for metastable systems, Phys. Rev. A **54**, 4770 (1996).

[41] G Nenciu and G Rasche, On the adiabatic theorem for nonself-adjoint Hamiltonians, J. Phys. A: Math. Gen. **25**, 5741 (1992).

[42] J. Höller, N. Read, and J. G. E. Harris, Non-Hermitian adiabatic transport in spaces of exceptional points, Phys. Rev. A **102**, 032216 (2020).

[43] N. Hatano and D. R. Nelson, Localization Transitions in Non-Hermitian Quantum Mechanics, Phys. Rev. Lett. **77**, 570 (1996).

[44] G. Salerno, T. Ozawa, H. M. Price, and I. Carusotto, Floquet topological system based on frequency-modulated classical coupled harmonic oscillators, Phys. Rev. B **93**, 085105 (2016).

[45] G. Salerno and I. Carusotto, Dynamical decoupling and dynamical isolation in temporally modulated coupled pendulums, Europhys. Lett. **106**, 24002 (2014).

[46] Y. Aharonov and D. Bohm, Significance of electromagnetic potentials in the quantum theory, Phys. Rev. **115**, 485 (1959).

[47] V. V. Konotop, J. Yang, and D. A. Zezyulin, Nonlinear waves in $\mathcal{PT}$-symmetric systems, Rev. Mod. Phys. **88**, 035002 (2016).

[48] Y. Lumer, Y. Plotnik, M. C. Rechtsman, and M. Segev, Nonlinearly Induced PT Transition in Photonic Systems, Phys. Rev. Lett. **111**, 263901 (2013).

[49] S. Yao, F. Song, and Z. Wang, Non-Hermitian Chern Bands, Phys. Rev. Lett. **121**, 136802 (2018).

[50] F. K. Kunst, E. Edvardsson, J. C. Budich, and E. J. Bergholtz, Biorthogonal Bulk-Boundary Correspondence in Non-Hermitian Systems, Phys. Rev. Lett. **121**, 026808 (2018).

[51] K. Kawabata, K. Shiozaki, and M. Ueda, Anomalous helical edge states in a non-Hermitian chern insulator, Phys. Rev. B **98**, 165148 (2018).